Preprint typeset in JHEP style - HYPER VERSION

Global fits of the Non-Universal Higgs Model

Leszek Roszkowski

Department of Physics and Astronomy, University of Sheffield,
Sheffield S3 7RH, UK,
and The Andrzej Soltan Institute for Nuclear Studies, Warsaw, Poland
E-mail: `L.Roszkowski@sheffield.ac.uk`

Roberto Ruiz de Austri

Instituto de Física Corpuscular, IFIC-UV/CSIC,
Valencia, Spain
E-mail: `rruiz@ific.uv.es`

Roberto Trotta

Astrophysics Group, Imperial College London
Blackett Laboratory, Prince Consort Road, London SW7 2AZ, UK E-mail:
`r.trotta@imperial.ac.uk`

Yue-Lin Sming Tsai

Department of Physics and Astronomy, University of Sheffield,
Sheffield S3 7RH, UK E-mail: `php06yt@sheffield.ac.uk`

Tom A. Varley

Department of Physics and Astronomy, University of Sheffield,
Sheffield S3 7RH, UK E-mail: `php06tav@sheffield.ac.uk`

Abstract: We carry out global fits to the Non-Universal Higgs Model (NUHM), applying all relevant present-day constraints. We present global probability maps for the NUHM parameters and observables (including collider signatures, direct and indirect detection quantities), both in terms of posterior probabilities and in terms of profile likelihood maps. We identify regions of the parameter space where the neutralino dark matter in the model is either bino-like, or else higgsino-like with mass close to 1 TeV and spin-independent scattering cross section $\sim 10^{-9} - 10^{-8}$ pb. We trace the occurrence of the higgsino-like region to be a consequence of a mild focusing effect in the running of one of the Higgs masses, the existence of which in the NUHM we identify in our analysis. Although the usual bino-like neutralino is more prominent, higgsino-like dark matter cannot be excluded, however its significance strongly depends on the prior and statistics used to assess it. We note that, despite experimental constraints often favoring different regions of parameter space to the Constrained MSSM, most observational consequences appear fairly similar, which will make it challenging to distinguish the two models experimentally.

Keywords: Supersymmetric Effective Theories, Cosmology of Theories beyond the SM, Dark Matter.

Contents

1. Introduction

Softly broken low-energy supersymmetry (SUSY) has many attractive features [1]. For example, unlike the Standard Model (SM), it provides an elegant solution to the gauge hierarchy problem and a natural weakly-interacting dark matter (DM) candidate, in addition to accounting for gauge coupling unification. On the other hand, SUSY itself has to be (softly) broken in order to make contact with reality, which in the general Minimal Supersymmetric Standard Model (MSSM) introduces a large number of new free parameters, namely the soft masses. Because of SUSY's natural link with grand unification theories (GUTs), one often explores SUSY models by imposing various boundary conditions at the GUT scale. The most popular model of this class is the Constrained MSSM (CMSSM) [2], in which not only do gaugino soft masses unify to $m_{1/2}$ but also soft masses of all the sfermions and Higgs doublets unify to m_0. These parameters, along with a common trilinear mass parameter A_0 and the ratio of Higgs vacuum expectation values $\tan\beta$, form the four continuous parameters of the CMSSM. The relative simplicity of the model makes a very attractive playground for many studies.

On the other hand, precisely because of its economy, the CMSSM may be missing some features of unified models with less restrictive boundary conditions at the unification scale. In particular, the assumption of Higgs (soft) mass unification with those of the sfermions does not seem strongly motivated since the Higgs and matter fields belong to different supermultiplets. One explicit example where this is the case is a minimal $SO(10)$ supersymmetric model (MSO$_{10}$SM) [3], which is well motivated and opens up a qualitatively new region of parameter space [4]. Models like this provide a good motivation for exploring a wider class of phenomenological models in which the soft masses m_{H_u} and m_{H_d} (as defined at the GUT scale) of the two Higgs doublets are treated as independent parameters and which come under the name of the Non-Universal Higgs Model (NUHM) [5]. [1]

We assume, as ever, a Minimal Flavor Violating (MFV) scenario with no additional flavor violating terms appearing beyond the SM ones. In the NUHM, there are therefore six continuous free parameters:

$$m_0, m_{1/2}, \tan\beta, A_0, m_{H_u} \text{ and } m_{H_d}. \tag{1.1}$$

The Renormalization Group Equations (RGEs) are then used to evaluate masses and couplings at the electroweak scale and the Higgs potential is minimized in the usual way. Electroweak Symmetry Breaking (EWSB) conditions for NUHM read:

$$\mu^2 = \frac{m_{H_d}^2 - m_{H_u}^2 \tan^2\beta}{\tan^2\beta - 1} - \frac{1}{2}m_Z^2, \tag{1.2}$$

$$m_A^2 = m_{H_d}^2 + m_{H_u}^2 + 2\mu^2, \tag{1.3}$$

where m_A stands for the mass of the pseudoscalar Higgs A and μ is the SUSY-preserving Higgs/higgsino mass parameter. In the above equations all the parameters are evaluated at the usual electroweak scale $M_{\rm SUSY} \equiv \sqrt{m_{\tilde{t}_1} m_{\tilde{t}_2}}$ (where $m_{\tilde{t}_1,\tilde{t}_2}$ denote the masses of the scalar partners of the top quark), chosen so as to minimize higher order loop corrections. At $M_{\rm SUSY}$ the (1-loop corrected) conditions of EWSB are imposed and the SUSY spectrum is computed at m_Z.

Like in the CMSSM the sign of μ remains undetermined. On the other hand, in contrast to the CMSSM, because of the larger number of free parameters Eqs. (1.2) and (1.3) allow one to treat both μ and m_A as independent parameters in place of high scale parameters m_{H_u} and m_{H_d}. This will have an important impact on the properties of the model. In particular, the ability to effectively choose the position of the A funnel or to tune μ for a given point in the parameter space to give a correct relic abundance of the neutralino DM will lead to very different phenomenological predictions, as we will see below.

The moderately increased number of free parameters of the NUHM has been shown to lead to a rich and distinct phenomenology (see, for example [8, 9, 10, 11] and references therein). In particular, there is a larger variety of choices for the lightest superpartner (LSP). In the CMSSM the LSP is either the lightest neutralino or the lighter stau or, in some relatively rare cases, the lighter stop. In contrast, in the NUHM, the LSP can in addition be a sneutrino or right handed selectron [9]. In this, as in previous analyses, we do not consider the possibility of a gravitino LSP. Assuming the LSP to be the dark matter in the Universe eliminates states that are not electrically neutral and leads to a non-trivial constraint on the parameter space. However, the near degeneracy of many states with the LSP leads to a great variety of co-annihilation channels. Also, given that m_A can now be treated effectively as a free parameter, the resonance channel can be important in different ways from the CMSSM. Also, as we will see, there are sizable regions of the

[1] A reduced version of NUHM with $m_{H_u} = m_{H_d}$ has also been examined in several papers, eg [6, 7].

parameter space where the neutralino is actually higgsino-like while giving the correct dark matter abundance. Such regions cannot be excluded although their statistical significance is presently difficult to determine, as we will show. Although in general a higgsino-dominated LSP in the mass range of several hundred GeV, or less, underproduces dark matter [12], as its mass increases the transition to higgsino dark matter can provide an acceptable relic density. In general these effects will be important to give the correct relic density in different parts of the parameter space of the model.

The larger number of parameters makes a full exploration of the NUHM parameter space even more challenging than that of the CMSSM. There are several important reasons why it might be advantageous to adopt a Markov Chain Monte Carlo (MCMC) sampling technique to perform a global scan, as we do in the present paper. First, fixed grid scans of the likelihood become rapidly inefficient with the increase of the dimensionality of the model's parameter space, as the computational effort required scales exponentially with the number of dimensions of the parameter space. Secondly, typically such scans do not have sufficient resolution to map out in detail the finer structure of the likelihood surface. The combination of those two aspects means that fixed grid scans are typically limited to exploring 2-dimensional slices of the likelihood at the time, while fixing all other parameters to arbitrary values. This leads to a large underestimation of the uncertainty in the parameters one is interested in studying and to limiting the ability to perform global scans of the model's parameter space. For example, fixed-grid scans identify in the CMSSM so-called "WMAP strips" in various 2-dimensional slices, i.e., tightly constrained regions of parameter space where the relic abundance is in good agreement with the WMAP value. However, the use of global scans which fit all model parameters simultaneously allows one to reveal that such strips only arise because the other parameters of the model (typically, A_0 and $\tan\beta$) have been fixed at arbitrary values. Once those quantities are incorporated in a global scan, the WMAP strips disappear and become unified in much wider error regions.

Recently, such difficulties have been overcome thanks to the introduction of MCMC scanning techniques coupled to Bayesian statistics (for recent studies of the CMSSM, see [13, 14]).[2] This methodology presents several significant advantages – as the computational effort of MCMC scales approximately linearly with the number of dimensions being scanned, all relevant parameters can be included simultaneously in the fit. This allows one to incorportate important residual uncertainties in the SM parameters, as well. The more efficient exploration of the likelihood allows one to efficiently explore regions of the models parameters that are not easily accessible in the usual fixed-grid scans. Another important aspect of the technique being used here is that, once the samples from the posterior have been accumulated, one can investigate both Bayesian maps (in terms of posterior distributions) and frequentist ones (the profile likelihood), in order to assess the robustness of the result with respect for example to different priors or choices of statistics. Whenever we consider the profile likelihood, we have of course removed the prior weight and are therefore effectively showing samples from the likelihood alone. Finally, it becomes

[2]An alternative χ^2-based approach has been pursued in Ref. [15].

possible to produce probability maps of any derived quantity that one is interested in, and of its correlations with any other variable of interest. Altogether, those advantages make MCMC methods a powerful tool for the global exploration of the NUHM parameter space.

In this paper we investigate global fits of the NUHM parameter space with a modified version of the `SuperBayeS` package [16]. Our fits include all the relevant constraints coming from experiment, in particular, the branching ratio of $b \to s\gamma$, the difference $\delta(g-2)_\mu$ between the experimental and SM values of the magnetic moment of the muon, the LEP limits on sparticle and Higgs masses, the 5 year WMAP limits on the relic density $\Omega_{\rm CDM}h^2$ and several other measured but imprecisely known quantities that SUSY can contribute to. It should be noted that we take a wider range of parameters than previous scans in the literature (up to 4 TeV in the case of the soft masses), and the MCMC technique allows us to vary all our parameters such that we also consider $A_0 \neq 0$, while at the same time varying relevant SM parameters. As our statistical measures we will apply a Bayesian posterior probability density function and profile likelihood, both to be introduced below.

The paper is organised as follows. In sec. 2 we summarise the statistical formalism that we employ and list the constraints that we apply in our numerical analysis. Next, in sec. 3 we present the constraints on NUHM parameters resulting from our global scan and discuss the main features, including the possibility of higgsino DM and a mild focusing effect. We also discuss some implications for phenomenology, including direct and indirect SUSY searches in colliders, while in sec. 4 we discuss prospects of direct and indirect detection of the neutralino dark matter in the model. We conclude and summarize our results in sec. 5. We also illustrate the prior dependence of some of our results in Appendix A.

2. Outline of the statistical treatment

In comparison to earlier analyses of the CMSSM [13, 14, 17] here we have a larger base parameter set, defined by

$$\theta = (m_{1/2}, m_0, A_0, \tan\beta, m_{H_u}, m_{H_d}), \tag{2.1}$$

where we fix sgn(μ)$=+1$. As the relevant SM parameters, when varied over their experimental ranges, have impact on the observable quantities, fixing them at their central values would lead to inaccurate results. Instead, here we incorporate them explicitly as free parameters (which are then constrained using their measured values), which we call *nuisance parameters* ψ, where

$$\psi = (M_t, m_b(m_b)^{\overline{MS}}, \alpha_{em}(m_Z)^{\overline{MS}}, \alpha_s(m_Z)^{\overline{MS}}). \tag{2.2}$$

In Eq. (2.2) M_t denotes the pole top quark mass, while the other three parameters: $m_b(m_b)^{\overline{MS}}$ – the bottom quark mass evaluated at m_b, $\alpha_{\rm em}(M_Z)^{\overline{MS}}$ and $\alpha_s(M_Z)^{\overline{MS}}$ – respectively the electromagnetic and the strong coupling constants evaluated at the Z pole mass m_Z - are all computed in the $\overline{MS}$ scheme. Using notation consistent with previous analyses we define our now ten *basis parameters* as

$$m = (\theta, \psi) \tag{2.3}$$

which we will be scanning simultaneously with the MCMC technique. For each choice of m various colliders or cosmological observables will be calculated. These derived variables are denoted by $\xi = (\xi_1, \xi_2, \ldots)$, which are then compared with the relevant available data d. The quantity we are interested in is the *posterior probability density function* (pdf), or simply posterior, $p(m|d)$ which gives the probability of the parameters after the constraints coming from the data have been applied. The posterior follows from Bayes' theorem,

$$p(m|d) = \frac{p(d|\xi)\pi(m)}{p(d)}, \tag{2.4}$$

where $p(d|\xi)$, taken as a function of ξ for *fixed data* d, is called the *likelihood* (where the dependence of $\xi(m)$ is understood). The likelihood is the quantity that compares the data with the derived observables. $\pi(m)$ is the *prior* which encodes our state of knowledge of the parameters before comparison with the data. This state of knowledge is then updated by the likelihood to give us the posterior. $p(d)$ is called the *evidence* or *model likelihood*, and in our analysis can be treated as a normalisation and hence is ignored subsequently. (See instead [18] for an example of how the evidence can be used for model comparison purposes.)

Our inference problem is fully defined once we specify the prior on the rhs of Bayes' theorem Eq. (2.4). We present our main results below for the following choice of priors (which we call our *log prior* case): a uniform prior on $\log m_{1/2}$, $\log m_0$, $\log m_{H_u}$ and $\log m_{H_d}$, in the range 50 GeV $< m_0, m_{1/2} <$ 4 TeV and $0 < m_{H_u}, m_{H_d} <$ 4 TeV, and a uniform prior on A_0 and $\tan\beta$ in the ranges $|A_0| <$ 7 TeV and $2 < \tan\beta < 62$. Notice that by this range of m_{H_u} and m_{H_d}, and taking $\mathrm{sgn}(\mu) > 0$, we automatically satisfy the GUT stability constraint of ref. [9].

Our choice of a prior uniform in the log of the masses is dictated by both physical and statistical reasons. From the physical point of view, log priors explore in much greater detail the low-mass region, which exhibits many fine-tuned points that can easily be missed otherwise. From the statistical point of view, log priors give the same *a priori* weight to all orders of magnitude in the masses, and thus appear to be less biased to giving larger statistical *a priori* weights to the large mass region, which under a flat prior has a much larger volume in parameter space.

In the ideal case where the likelihood is sharply peaked within the range of the prior, the posterior is dominated by the likelihood and the details of the prior choice do not matter. However, given present-day data even the CMSSM exhibits a certain amount of prior dependence [19], which is however expected to be strongly reduced once future LHC data become available [20]. We thus expect that the NUHM will also be affected by a certain amount of prior dependence. In order to assess whether our results are robust wrt the prior choice we also investigate a different statistical measure, namely the profile likelihood. It is obtained from our scan by maximising over the parameters not shown (rather than integrating over them, as one does to obtain the Bayesian posterior).[3]

The profile likelihood has the advantage of being a prior-independent quantity. However, it is a difficult quantity to evaluate numerically, for it requires a maximisation along

[3] The procedure for evaluating the profile likelihood that we use can be found in Ref. [19].

the directions one is profiling over. Therefore, it is very difficult to ensure that sparse-sampling schemes (such as MCMC) have gathered a sufficient number of samples to guarantee that the profile likelihood obtained from them can be deemed to be stable and robust. We stress that the MCMC algorithm we adopt in our study is not designed to achieve a maximisation of the likelihood – rather, the MCMC exploration is targeted at obtaining samples from modes of large posterior mass. This is of special concern for multi-dimensional parameter spaces with a fragmented, multi-modal likelihood function such as the one being considered here. Indeed, the analysis of Ref. [21] showed that a genetic algorithm can be used to find better fitting points than those returned by MCMC (albeit with a computational effort which is about 10 times larger). Related statistical issues in connection with profile likelihood coverage properties have also been recently discussed in [22]. Since profile likelihood confidence intervals depend on the value of the best fit likelihood, this implies that the results we present below for profile likelihood intervals have to be interpreted with great caution. In particular, the best-fit points we report below (and their χ^2 values) should be considered as representative of the the various physical regions in parameter space, rather than the absolute global best fits. The aim of this work is to achieve a first global exploration of the NUHM, and therefore we leave the detailed discussion of the stability of the profile likelihood reconstruction from MCMC methods to a future, dedicated study [23].

In fact, the profile likelihood and the Bayesian posterior ask two different statistical questions of the data: the latter evaluates which regions of parameter space are most plausible in the light of the measure implied by the prior (and is thus in general prior dependent except when the data are sufficiently constraining to overrule any sensible choice of prior); the former singles out regions of high quality of fit, independently of their extent in parameter space and of the prior choice, thus disregarding the possibility of them being highly fine-tuned. The information contained in both is relevant and interesting in evaluating the viability of the underlying physical properties of the model (possible collider signatures, etc) which of course do not depend on our statistical tools *per se*. However, our conclusions about the plausibility of such physical properties might be different depending on the exact statistical question asked of the data, e.g., whether one considers a posterior pdf or a profile likelihood (in the simple case of a Gaussian distributed quantity, both the pdf and the profile likelihood are identical and thus the question of which to choose does not arise). In Appendix A we examine the robustness of our results with respect to a change of priors in the mass variables.

The SM parameters are assigned flat priors over a sufficiently wide range and are then constrained by applying Gaussian likelihoods representing the experimental observations (see table 1). The Gaussian likelihoods being much more sharply peaked than the flat prior range, we find that the posterior is completely dominated by the likelihood for the SM parameters.

The predictions for the observable quantities are obtained by using SoftSusy 2.0.5 and DarkSusy 4.0 [24, 25] as implemented in the `SuperBayeS` code. The likelihoods for the relevant observables are taken as Gaussian (for measured observables) with mean μ, experimental errors σ and theoretical errors τ (see the detailed explanation in [14]). In

SM (nuisance) parameter	Mean value μ	Uncertainty σ (exper.)	ref.
M_t	172.6 GeV	1.4 GeV	[28]
$m_b(m_b)^{\overline{MS}}$	4.20 GeV	0.07 GeV	[29]
$\alpha_s(M_Z)^{\overline{MS}}$	0.1176	0.002	[29]
$1/\alpha_{\rm em}(M_Z)^{\overline{MS}}$	127.955	0.018	[29]

Table 1: Experimental mean μ and standard deviation σ adopted for the likelihood function for SM (nuisance) parameters, assumed to be described by a Gaussian distribution.

Observable	Mean value	Uncertainties		ref.
	μ	σ (exper.)	τ (theor.)	
m_W	80.392 GeV	29 MeV	15 MeV	[30]
$\sin^2\theta_{\rm eff}$	0.23153	16×10^{-5}	15×10^{-5}	[30]
$\delta(g-2)_\mu \times 10^{10}$	27.5	8.4	1	[31]
$BR(\overline{B} \to X_s\gamma) \times 10^4$	3.55	0.26	0.21	[32]
ΔM_{B_s}	17.33 ps^{-1}	0.12 ps^{-1}	4.8 ps^{-1}	[33]
$\Omega_\chi h^2$	0.1099	0.0062	$0.1\,\Omega_\chi h^2$	[34]
	Limit (95% CL)		τ (theor.)	ref.
$BR(\overline{B}_s \to \mu^+\mu^-)$	$< 5.8 \times 10^{-8}$		14%	[35]
m_h	> 114.4 GeV (91.0 GeV)		3 GeV	[36]
ζ_h^2	$f(m_h)$		negligible	[36]
sparticle masses	See table 4 in ref. [14].			

Table 2: Summary of the observables used in the analysis. Upper part: Observables for which a positive measurement has been made. $\delta(g-2)_\mu$ denotes the discrepancy between the experimental value and the SM prediction of the anomalous magnetic moment of the muon $(g-2)_\mu$. For central values of the SM input parameters used here, the SM value of $BR(\overline{B} \to X_s\gamma)$ is 3.11×10^{-4}, while the theoretical error of 0.21×10^{-4} includes uncertainties other than the parametric dependence on the SM nuisance parameters, especially on M_t and $\alpha_s(M_Z)^{\overline{MS}}$. For each quantity we use a likelihood function with mean μ and standard deviation $s = \sqrt{\sigma^2 + \tau^2}$, where σ is the experimental uncertainty and τ represents our estimate of the theoretical uncertainty (see [14] for details). Lower part: Observables for which only limits currently exist. The likelihood function is given in ref. [14], including in particular a smearing out of experimental errors and limits to include an appropriate theoretical uncertainty in the observables. m_h stands for the light Higgs mass while $\zeta_h^2 = g^2(hZZ)_{\rm MSSM}/g^2(hZZ)_{\rm SM}$, where g stands for the Higgs coupling to the Z and W gauge boson pairs.

the case where there only an experimental limit is available, this is given, along with the theoretical error. The smearing out of bounds and combination of experimental and theoretical errors is handled in an identical manner to [14].

Any points that fail to provide radiative EWSB, give us tachyonic sleptons or provide the LSP which is not the lightest neutralino are excluded. As in previous works [14, 17, 26], we adopt a Metropolis-Hastings MCMC algorithm to sample the parameter space. We have also cross-checked our results by employing the more recently implemented MultiNest algorithm [27, 19] and the findings are compatible (up to numerical noise). The results presented in the rest of this paper are obtained from the 25 chains that were used, garnering a total of 3×10^5 samples each, with an acceptance rate of around 4%. Convergence criteria are the same as in our previous papers [14, 17, 26].

3. Global constraints on NUHM parameters

In this section we present some results from our global scans of the NUHM parameter space.

3.1 Probability maps of NUHM parameters

To start with, in the top row of fig. 1 we plot joint 2D posteriors for some combinations of the NUHM base parameters, marginalising over the parameters not shown. In the bottom row, we plot instead the profile likelihood, where the other parameters have been maximised over. In terms of the posterior pdf, we can see that the 68% probability region (inner contour) for $m_{1/2}$ and m_0 is remarkably well confined to mostly a fairly low mass region of $m_{1/2} \lesssim 1$ TeV and $m_0 \lesssim 1.4$ TeV, where also the overall best fit point, marked by a blue triangle is located (see below for further discussion). However, the 95% posterior region (outer contour) is much wider and extends to much larger ranges of both parameters. This signals that the constraining power of the data is not sufficient to strongly confine the posterior. Turning to the middle panel, we can see a preference for moderately large $\tan\beta \lesssim 40$, as well as for positive A_0, although zero or negative values of A_0 are not excluded. Finally, regarding the new parameters beyond the CMSSM, we see that m_{H_u} is fairly poorly constrained while m_{H_d} favors rather low values, ~ 1 TeV at 95% probability.

It is worth comparing the posterior regions of the NUHM with those for the analogous parameters in the CMSSM. The two top left panels in fig. 1 are directly comparable with the corresponding bottom panels in Fig. 13 of [19] for the CMSSM. It is clear that, while in both the CMSSM and the NUHM high probability regions are given by rather low $m_{1/2}$ and m_0 (assuming the log prior, see Appendix A for further comments on prior dependence), but actually they are different and favored by different physical mechanisms. As is well known, in the CMSSM this is mostly the neutralino-stau coannihilation region of $m_0 \ll m_{1/2} \lesssim 1$ TeV [19] (plus a tiny vertical region of Z and h pole annihilation), while in the NUHM the analogous (mentioned above) “low-mass” ranges $m_{1/2} \lesssim 1$ TeV and $m_0 \lesssim 1.4$ TeV corresponds to the “bulk region” where A funnel annihilation play a dominant rôle. In both models, the favored ranges (and also best fit points) of $\tan\beta$ are rather moderate (although in the CMSSM very large values of around 55 are also allowed at 68%, in contrast to the NUHM). Finally, A_0 in both models shows a mild preference for positive values but otherwise is not well constrained. Also shown in fig. 1 (as triangles) are the best-fit points corresponding to the different regions divided by three different neutralino DM compositions: mostly gaugino ($Z_g > 0.7$), mixed ($0.7 < Z_g < 0.3$) and mostly higgsino ($Z_g < 0.3$), where $Z_g = Z_{11}^2 + Z_{12}^2$ and Z_{11}^2 and Z_{12}^2 are the respective bino and wino fractions. We will come back to this point below when we discuss dark matter aspects of the model.

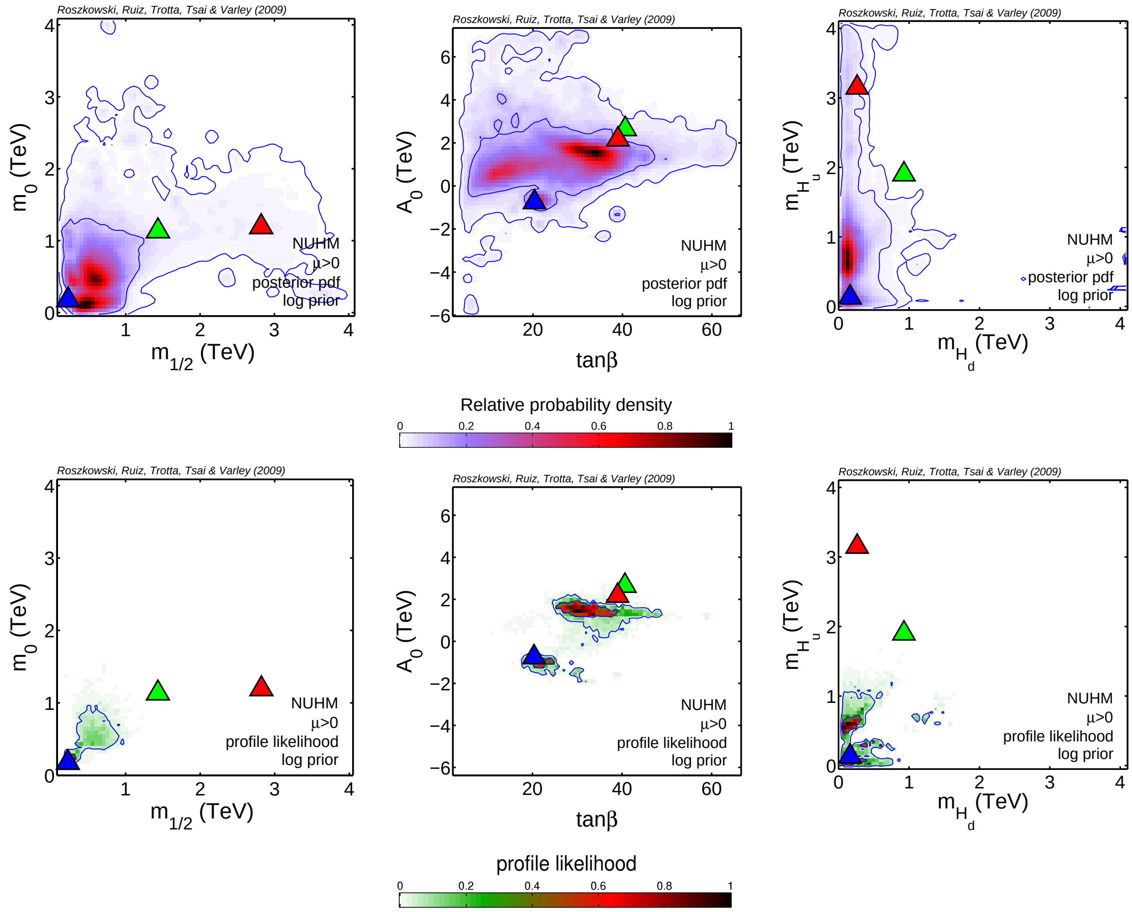

Figure 1: Top panels: the 2D posterior for the log prior choice in the planes spanned by three pairs of NUHM parameters: $(m_{1/2}, m_0)$, $(\tan\beta, A_0)$ and (m_{H_d}, m_{H_u}) for $\mu > 0$. The inner (outer) blue solid contours delimit regions encompassing 68% and 95% of the total posterior probability, respectively. Triangles mark the location of the best-fit points for each of the three different DM compositions: mostly gaugino (blue), mostly higgsino (red) and mixed (green); see text for details. The overall best-fit is the blue triangle, see Table 3 and discussion below. Bottom panel: profile likelihood maps for the same quantities, where all other parameters have been maximised over. Contours denote 68% and 95% confidence regions from the profile likelihood.

Turning now to the profile likelihood maps (bottom panels of Fig. 1, we see that the confidence contours from this statistical measure are much more strongly confined than the posterior. The favoured region at 95% from the profile likelihood is always inside the 68% posterior region obtained from the posterior. This constraints all of the NUHM soft masses to be below ~ 1 TeV, with A_0 confined within ± 2 TeV around zero and moderate values of $\tan\beta$ between some 20 and 40 being preferred. This striking difference between the posterior and the profile likelihood can be understood with the help of Fig. 2 which investigates some of the observables that play a key rôle in determining the favored regions of NUHM parameter space using either statistics, namely the neutralino relic abundance $\Omega_\chi h^2$, $BR(\overline{B} \to X_s\gamma)$, the SUSY contribution to $(g-2)_\mu$ and the light Higgs mass m_h. The

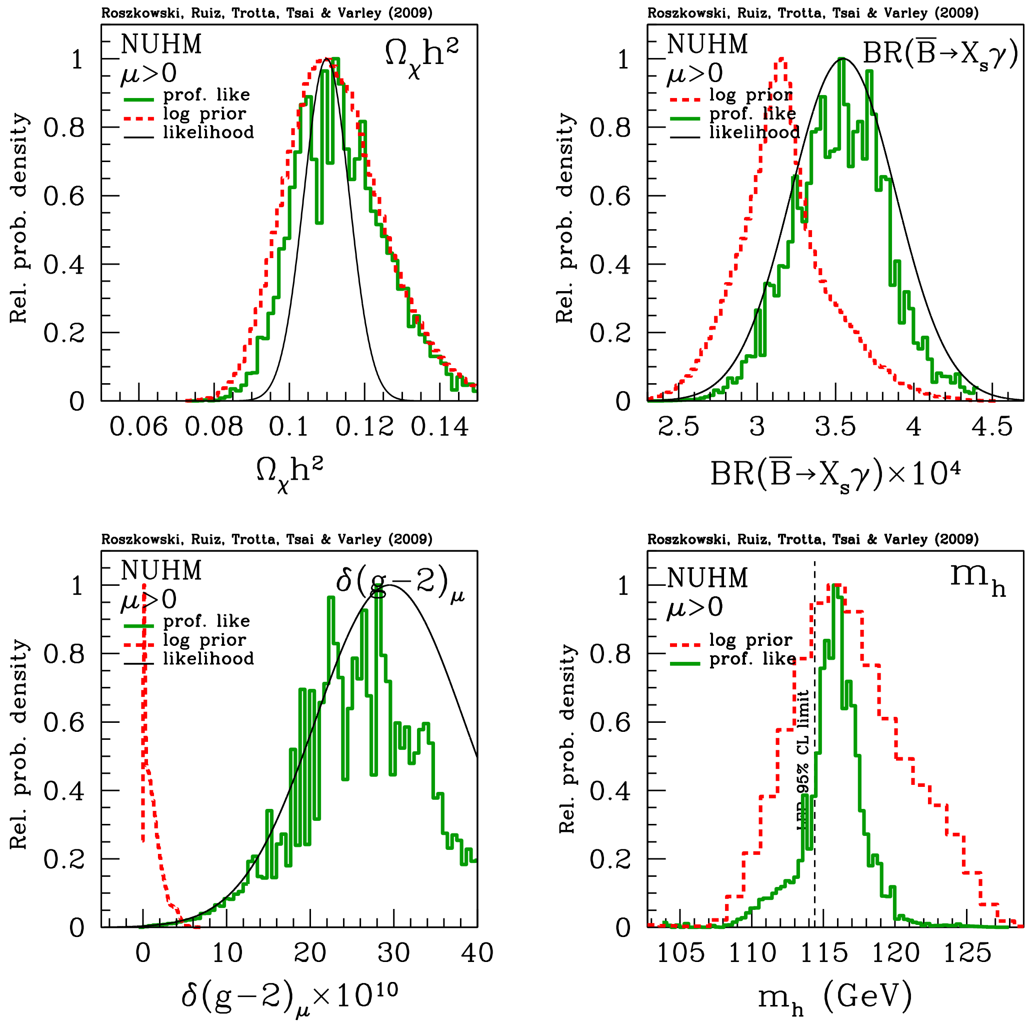

Figure 2: The 1D posterior probability density (red, from our log prior scan) and the profile likelihood (green) for $\Omega_\chi h^2$ (upper left panel), $BR(\overline{B} \to X_s\gamma)$ (upper right panel), $\delta(g-2)_\mu$ (lower left panel) and the light Higgs mass m_h (lower right panel). In each panel we also plot the the likelihood function used to constrain the observable (solid black).

tight WMAP constraint on $\Omega_\chi h^2$ in the likelihood is well matched by the shape of the 1D pdf as well as by the profile likelihood, showing that this particular observable can be well fitted in the model. On the contrary, we observe a certain discrepancy between the 1D pdf of $BR(\overline{B} \to X_s\gamma)$ and the likelihood function. The posterior shows a rather strong preference for what is basically the SM value of the observable. The same effect can be seen in the posterior for $(g-2)_\mu$, which is strongly peaked at very small values. Both those effects are a consequence of the fact that, under the prior measure chosen, the vast majority of points in the NUHM parameter space leads to a prediction for $BR(\overline{B} \to X_s\gamma)$ and $(g-2)_\mu$ which

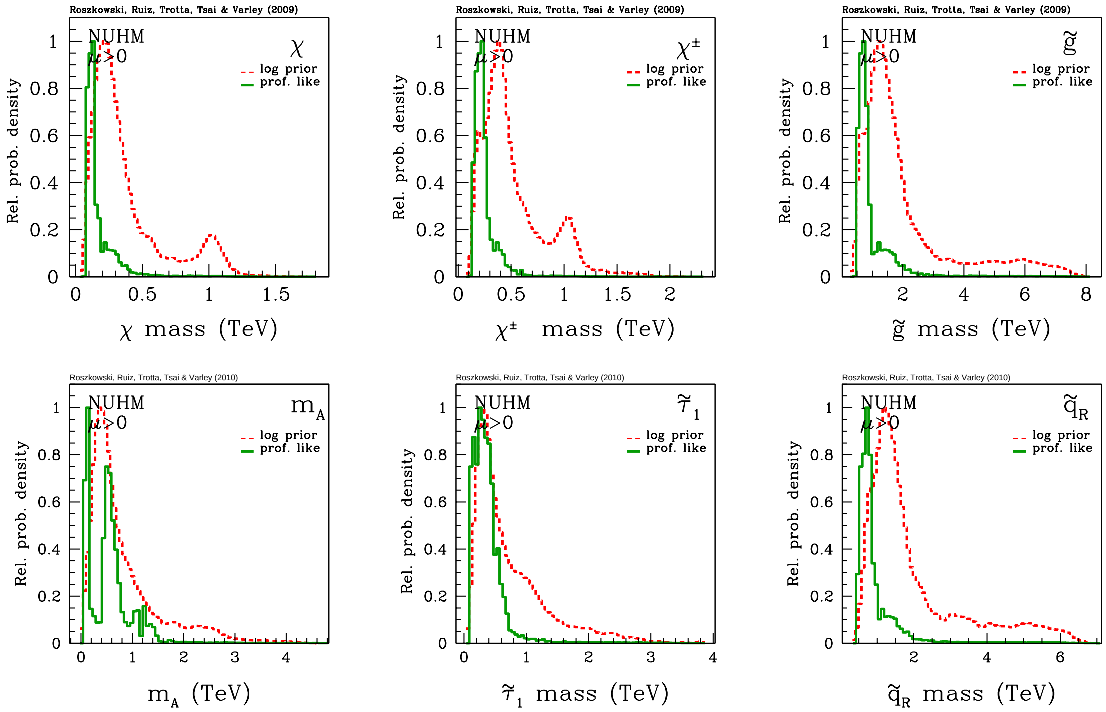

Figure 3: Top row: The 1D posterior probability and the profile likelihood for the lightest neutralino mass m_χ (left panel), the lightest chargino $m_{\chi_1^\pm}$ (middle panel) and the gluino $m_{\tilde{g}}$ (right panel). Bottom row: the same quantities for the mass of the lightest neutralino m_A (left panel), the first stau $m_{\tilde{\tau}_1}$ (middle panel) and a squark $m_{\tilde{q}_r}$ (right panel).

is very close to their SM value. The likelihood function is not strong enough to completely override this preference, and hence the posterior remains influenced by the prior. This statistical effect has already been noticed in the case of the CMSSM [37, 26, 19]. The profile likelihood for $BR(\overline{B} \to X_s\gamma)$ and $(g-2)_\mu$ instead follows closely the values of the likelihood function. This shows that there are indeed a small number of samples in our chains which achieve both the correct $BR(\overline{B} \to X_s\gamma)$ and $(g-2)_\mu$ values. As we shall show below, it is in fact the $(g-2)_\mu$ constraint that mostly drives the fit. However, since the number of the samples which provide a good fit to both observables is so small, their posterior probability is suppressed, as in Bayesian statistics points that are finely tuned wrt the prior measure are penalized. We therefore conclude that the tight constraints on the NUHM parameters obtained from the profile likelihood are largely driven by the need to fit both $BR(\overline{B} \to X_s\gamma)$ and $(g-2)_\mu$, two observables that appear to be in some tension [38].

Finally, the posterior for m_h still allows fairly low values of the Higgs mass. Interesting, unlike in the CMSSM, the lightest Higgs is not necessarily SM-like and therefore the 95% LEP lower bound on SM Higgs mass should only be considered as indicative. In fact, our analysis fully accounts for the possibility of non SM-like Higgs in the likelihood. The same conclusion remains qualitatively valid even in terms of the profile likelihood statistics.

Moving on to the sparticle spectrum of the best-fit point, we present in the top row of fig. 3 the 1D posterior and profile likelihood for the lightest neutralino (left panel), the lighter chargino (middle panel) and the gluino (right panel). In each case, the secondary bump observed in the posterior at $m_\chi \sim 1$ TeV, $m_{\chi_1^\pm} \sim 1$ TeV and $m_{\tilde{g}} \sim 6$ TeV is a reflection of the parameter space region leading to higgsino DM, as we will discuss in detail below. In the bottom row, we show the posterior and profile likelihood for the pseudoscalar Higgs and sleptons. The non-universality of m_{H_u} and m_{H_d} in the NUHM can lead to a large positive value for the S parameter, defined in the RGEs as: $S = m_{H_u}^2 - m_{H_d}^2 + \mathrm{Tr}\left[\mathbf{m_Q^2} - \mathbf{m_L^2} - \mathbf{2m_{\bar{u}}^2} + \mathbf{m_{\bar{d}}^2} + \mathbf{m_{\bar{e}}^2}\right]$, where the parameters in boldface denote 3×3 soft mass parameters. In general the S parameter is a fixed point in the RGEs of the CMSSM, but in the NUHM it can be nonzero and make large contributions to the running of many of the scalars, leading to, for example several light sleptons. However, we do not find this to be the case.

The first column of Table 3 gives the best fit values for the NUHM base parameters and for a number of quantities of particular interest, as well as the overall χ^2 value and the pull of each observable. The dominant role of the $(g-2)_\mu$ constraint in driving the fit towards the small mass region will be discussed in more detail at the end of the next subsection where we examine the higgsino-dominated DM and address the question of its statistical viability.

3.2 Higgsino dark matter in the NUHM

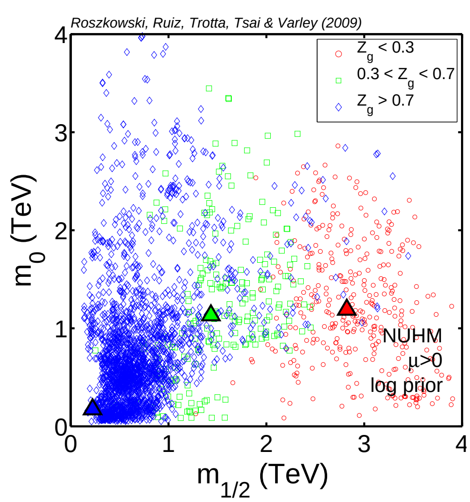

Figure 4: A distribution of the gaugino fraction Z_g in the plane of $(m_{1/2}, m_0)$ for samples uniformly selected from our MC chains. The color coding is as follows: red dots correspond to $Z_g < 0.3$ (mostly higgsino), green squares to $0.3 < Z_g < 0.7$ and blue diamonds to $Z_g > 0.7$ (mostly gaugino). The triangles denote the best fit point for each cloud of samples of a given respective gaugino fraction (of corresponding color) taken separately. The overall best-fit is in the gaugino-like DM region.

An interesting feature of the NUHM is the possibility of higgsino-like neutralino DM,

Z_g composition	$Z_g > 0.7$	$0.7 < Z_g < 0.3$	$Z_g < 0.3$
	Base parameters		
$m_{1/2}$	0.224 TeV	1.43 TeV	2.83 TeV
m_0	0.174 TeV	1.13 TeV	1.19 TeV
m_{H_u}	0.129 TeV	1.90 TeV	3.15 TeV
m_{H_d}	0.162 TeV	0.927 TeV	0.263 TeV
A_0	1.56 TeV	2.64 TeV	2.17 TeV
$\tan\beta$	20.4	40.6	39.0
	Observables		
$\Omega_\chi h^2$	0.111	0.112	0.108
Z_g	0.989	0.655	0.00256
m_χ	88.6 GeV	593 GeV	1.04 TeV
$m_\chi^\pm$	488 GeV	640 GeV	1.05 TeV
σ_p^{SI} (pb)	2×10^{-9}	1.44×10^{-7}	1.81×10^{-8}
	Annihilation channels		
$\langle\sigma_{ann}v\rangle$ (Dom.)	$\chi_1^0\chi_1^0 \to \tau\tau$ (57%)	$\chi_1^0\chi_1^0 \to t\bar{t}$ (15%)	$\chi_1^0\chi_1^+ \to u\bar{d}$(8%)
$\langle\sigma_{ann}v\rangle$ (Sub.)	$\chi_1^0\tilde{\tau}_1 \to A\tau$ (11%)	$\chi_1^0\chi_1^0 \to b\bar{b}$ (13%)	$\chi_1^0\chi_1^+ \to c\bar{s}$(8%)
	Pulls for observables		
$\chi^2_{\Omega_\chi h^2}$	< 0.01	0.04	0.03
χ^2_{Higgs}	0.84	0.08	< 0.01
$\chi^2_{\text{sparticles}}$	< 0.01	0.0	0.0
χ^2_{nuisance}	< 0.01	0.68	0.77
$\chi^2_{(g-2)_\mu}$	< 0.01	8.10	9.80
$\chi^2_{b\to s\gamma}$	< 0.01	0.08	0.06
$\chi^2_{m_W}$	0.56	1.42	1.22
$\chi^2_{\sin^2\theta_{\text{eff}}}$	0.36	0.06	0.05
$\chi^2_{\Delta M_{B_s}}$	< 0.01	0.16	0.23
	Quality of fit and parameter space fraction		
χ^2_{tot}	1.76	10.62	12.16
Parameter space	80.5%	7.4%	12.1%

Table 3: Best-fit points in each of the three different regions regarding the neutralino dominant composition: mostly gaugino ($Z_g > 0.7$), mixed ($0.7 < Z_g < 0.3$) and mostly higgsino ($Z_g < 0.3$) regions. The overall best-fit is in the gaugino region, where the neutralino is mostly bino (left column). The bottom section shows the corresponding χ^2 value and the parameter space fraction covered by each region.

as we have already mentioned above.[4] That this possibility exist in the NUHM should come as no surprise, since the μ parameter can now be chosen as a free parameter, and thus adjusted such as to give the correct amount of the relic density. On general ground, in order to satisfy this constraint in the MSSM-type models, the LSP neutralino must either

[4]The possibility of higgsino-like LSP in the NUHM has also been noticed in [39] but not explored in more detail.

be mostly bino-like (like in the CMSSM) if the bino soft mass $M_1 < |\mu|$, a sufficiently heavy higgsino-like state with $|\mu| < M_1$, or a mixed region in between the two.

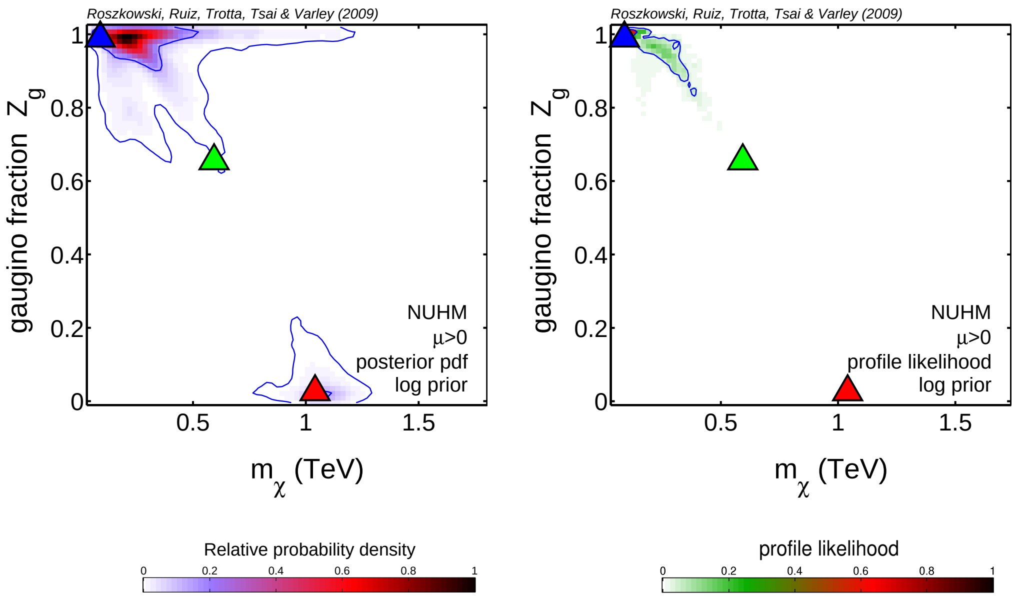

Figure 5: Left panel: Posterior probability distribution for the neutralino mass m_χ and its gaugino fraction Z_g. Right panel: corresponding profile likelihood. As above, triangles mark the location of the best-fit points for each of the three different DM compositions: mostly gaugino (blue), mostly higgsino (red) and mixed (green). The overall best-fit is given by the blue triangle.

On the other hand, it is not at all clear to what extent satisfying the relic abundance condition in a specific unified model like the NUHM is allowed by the other constraints that are currently available. This is an interesting issue, since the viability of the higgsino region in the NUHM could potentially lead to a phenomenological differences with the CMSSM, where the neutralino is mostly a bino.

To start with, in Fig. 4 we show in the plane $(m_{1/2}, m_0)$ a distribution of samples uniformly selected from our MC chains, which are color-coded according to the gaugino fraction Z_g of the lightest neutralino. Red circles correspond to a mostly higgsino state, $Z_g < 0.3$, green squares to a mixed state $(0.3 < Z_g < 0.7)$ and blue diamonds to mostly gaugino neutralino, $Z_g > 0.7$. Notice that, differently from usual "random scans" of the parameter space, in the case of Fig. 4 the density of samples reflects their relative posterior probability (as a consequence of them having been drawn using MCMC), hence we can make quantitative probabilistic statements about the relative viability of the different regions given our choice of prior.

The higgsino DM region corresponds to large values of $m_{1/2}$ (within the 2σ posterior contour in the left panel of Fig. 1). As $m_{1/2}$ becomes smaller, the bino-dominated fraction takes over, since in this region the neutralino mass is approximated by M_1, which scales with $m_{1/2}$. In between the two, we find a relatively smaller sample of mixed-type neutralino cases. The triangles denote the best fit point for each cloud of samples of a given respective gaugino fraction (of corresponding color) taken separately.

Fig. 5 shows the posterior pdf (left panel) and the profile likelihood (right panel) for the gaugino fraction of the neutralino *vs.*its mass. In the posterior distribution, the upper left island of probability corresponds to bino-like LSP, while the bottom right region around 1 TeV corresponds to the higgsino case. However, as mentioned above, the higgsino-like region is strongly disfavoured by the profile likelihood, as can be seen in the right panel. In this particular projection, the mixed region has too little statistical weight to be visible.

While the presence in the NUHM of a sizable region of parameter space where the LSP has a large higgsino fraction, as shown in Fig. 4, can easily be understood at the electroweak scale if one treats μ as a free parameter, it is interesting to investigate the underlying mechanism at the unification scale. Below we show that in the NUHM the appearance of the higgsino-like LSP is a consequence of an interesting feature of the model which is the existence of a mild focusing effect in the RG running of m_{H_u}, akin, but identical, to that in the CMSSM [40].

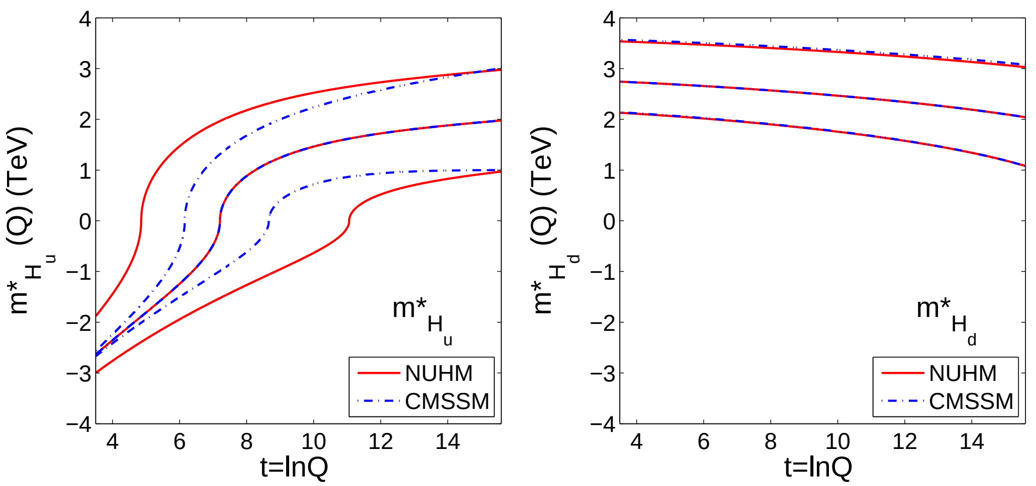

Figure 6: The running of $m^*_{H_u}(Q)$ (left panel) and $m^*_{H_d}(Q)$ (right panel) with the log of energy scale $t = \ln Q$. We take $A_0 = 4$ TeV, $m_{1/2} = 3$ TeV, $\tan\beta = 5$ and, in the NUHM case (red solid lines), $m_0 = 2$ TeV. In order to facilitate comparison with the CMSSM (blue dash-dotted lines), for each curve we initially set $m_{H_d} = m_{H_u}$ and then evolve differently for each model. In the CMSSM, for each curve we take $m_0 = m_{H_d} = m_{H_u}$, which is why the middle curves overlap.

For further discussion it will be convenient to introduce the running parameters $m^*_{H_u}(Q)$ and $m^*_{H_d}(Q)$, where Q is the energy scale, defined as

$$m^*_{H_{u,d}}(Q) = \mathrm{sgn}\left(m^2_{H_{u,d}}(Q)\right)\, |m^2_{H_{u,d}}(Q)|^{1/2}. \tag{3.1}$$

Since in the RGEs the running Higgs soft mass parameters $m_{H_u}(Q)$ and $m_{H_d}(Q)$ appear only in squares, which can become negative, the parameters $m^*_{H_{u,d}}(Q)$ are convenient to deal with in the sense that they adequately reflect both the magnitude and the sign of the respective parameters $m^2_{H_{u,d}}(Q)$. In particular, the quantities $m^*_{H_{u,d}}$, without any arguments, will denote the respective running quantities evaluated at $Q = M_{\rm SUSY}$,

$$m^*_{H_{u,d}} \equiv m^*_{H_{u,d}}(Q = M_{\rm SUSY}). \tag{3.2}$$

The focusing effect that we have identified is illustrated in fig. 6 where red solid lines show the running of the NUHM parameters $m^*_{H_u}(Q)$ (left panel) and $m^*_{H_d}(Q)$ (right panel) with the log of energy scale $t = \ln Q$. For each case we take $A_0 = 4$ TeV, $m_{1/2} = 3$ TeV and $\tan\beta = 5$. In order to facilitate comparison with the CMSSM (blue dash-dotted lines), for each curve we initially set $m_{H_d} = m_{H_u}$ and then evolve differently in each model. In the NUHM we fix also $m_0 = 2$ TeV while in the CMSSM, for each curve we take $m_0 = m_{H_d} = m_{H_u}$, which is why the curves in the middle case overlap. One can see that, in the NUHM the running of m_{H_u} is stronger for larger GUT values of the parameter, but it is not as strong as in the CMSSM.

As a result, we can see some "squeezing" of $m^*_{H_u}$ compared to the GUT values m_{H_u}, while this is not the case with the H_d soft mass parameter. This is shown in the left panel of Fig. 7 where islands of 68% posterior probability region of $m^*_{H_u}$ between some -1 TeV and -0.5 TeV (close to the location of the best fit points) correspond to large values of m_{H_u} (compare fig. 1), close to the assumed upper limit of the prior, nearly independently of the H_d soft mass parameter. It is clear that $m^*_{H_u}$ is to a large extent constrained by the focusing effect in the RG running. On the other hand, regions where m_{H_u} tends to be small correspond to a bino-like neutralino with the correct relic density, as we will show below. In this case, however, m_{H_d} is confined to preferably fairly small values ($\lesssim 2$ TeV), as otherwise one ends up with tachyonic sleptons. The corollary to this is that, in general we have more freedom in obtaining a phenomenologically desired range of values at the electroweak scale by appropriately choosing m_{H_u} at the GUT scale. Clearly that is not so in the CMSSM as one can never attain smaller μ here due to the stronger FP behaviour essentially focusing to nearly one point at the EW scale. The two distinct branches visible in the left panel of fig. 7 correspond to the two distinct neutralino regimes, as shown in the right panel of of the Figure. In the horizontal branch the neutralino is mostly a higgsino (red dots), turning into mixed (green squares) while the other, an inverted V-shaped region around $m^*_{H_d} = 0$ gives us a mostly bino (blue diamonds).

Above the reach of current collider limits, the high probability regions of m_{H_u}, m_{H_d} and the other soft parameters are primarily determined by requiring the correct dark matter abundance.[5] The higgsino case is obtained in the NUHM, because, as explained above, by starting with large enough m_{H_u} at the GUT scale one arrives, via the mild focusing effect (see fig. 6) at less negative values of $m^*_{H_u}$ at the EW scale. In the limit $|m^*_{H_d}| \ll |m^*_{H_u}|$ and large enough $\tan\beta$, Eq. (1.2) would imply $\mu \simeq |m^*_{H_u}|$. In reality, in the NUHM this limit is often violated and as a result μ comes out somewhat larger. On the other hand, $m_\chi \simeq |\mu|$ has to be large enough to give an acceptable relic density, as mentioned before. Numerically, this leads to $\mu \gtrsim 0.8$ TeV, which translates (via $0.4\, m_{1/2} \simeq M_1 > |\mu|$) to $m_{1/2} \gtrsim 2$ TeV. This explains the position of the broad higgsino region at large $m_{1/2}$ in Figs. 1 and 4. The second EWSB condition, Eq. (1.3), then implies the approximate relation $m_A^2 \simeq m^{*2}_{H_d} + \mu^2$ which we have checked numerically to hold.

[5]Exploratory runs with the constraint switched off yield much wider ranges of parameters.

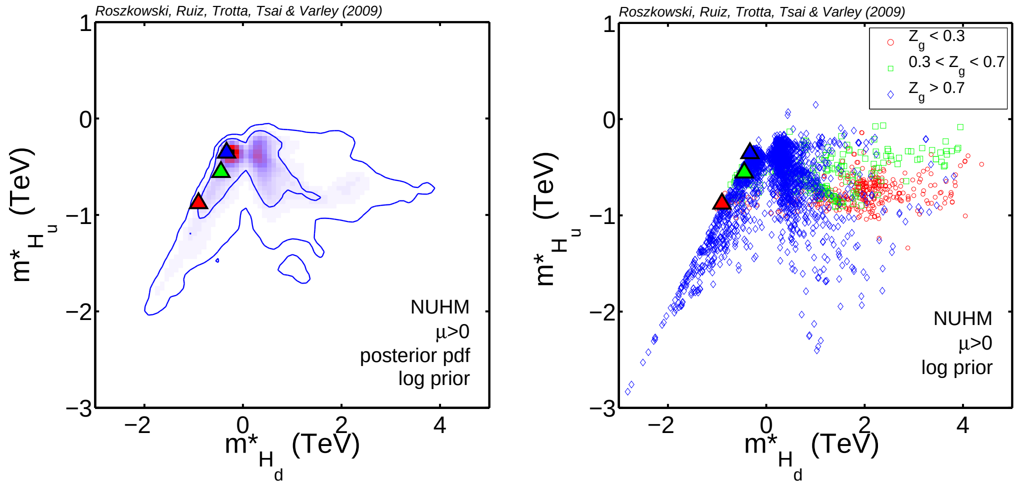

Figure 7: Left panel: posterior probability for $m^*_{H_u}$ and $m^*_{H_d}$, with the best-fit points for each of the three DM composition types marked by triangles as above. Right panel: A distribution of the gaugino fraction Z_g in the same plane of samples uniformly selected from our MC chains. The color coding is as before. The triangles denote the best fit point for each cloud of samples of a given respective gaugino fraction (of corresponding color) taken separately. The overall best-fit is in the gaugino-like DM region.

The condition $\mu \gtrsim 0.8$ TeV is reflected in the vertical red band (higgsino-like DM) in the left panel of Fig. 8 where we show the distribution of samples (color-coded according to the gaugino fraction) in the plane (m_χ, m_A). On the other hand, as μ increases, so does $\Omega_\chi h^2$ which quickly becomes unacceptably large. As a result one finds a strong concentration at $\mu \simeq 1$ TeV, corresponding to higgsino LSP (compare middle panel). On the other hand, the diagonal branch in fig. 8 corresponds to the second way of arriving at the correct relic density, namely via an A resonance annihilation of bino-like neutralino which is clearly also realized in the NUHM. In this case the LSP mass m_χ extends over a range of values and the correct relic density is achieved when $m_A \simeq 2m_\chi$, as one can clearly see in the left panel of fig. 8. On the other hand, there appear to be little correlation between m_A and μ (right panel of the Figure).

As we have seen, a great majority of viable points in our scans of the NUHM parameter space give bino-like DM, while it is the higgsino-like cases that could lead to a potentially striking distinction from the CMSSM. It is therefore worth assessing the statistical viability of higgsino DM in the NUHM.

In terms of posterior probability, the relative probability of each DM composition (mostly higgsino, mostly bino or mixed) can be determined by counting the number of independent samples of each type. We find that, under the assumption of the log prior, the probability of the higgsino region is $\sim 12\%$, while the gaugino region has a probability of $\sim 74\%$, as reported in Table 3. However, those results are expected to be prior-dependent, as we have already seen that the constraints do not appear to be sufficiently strong to

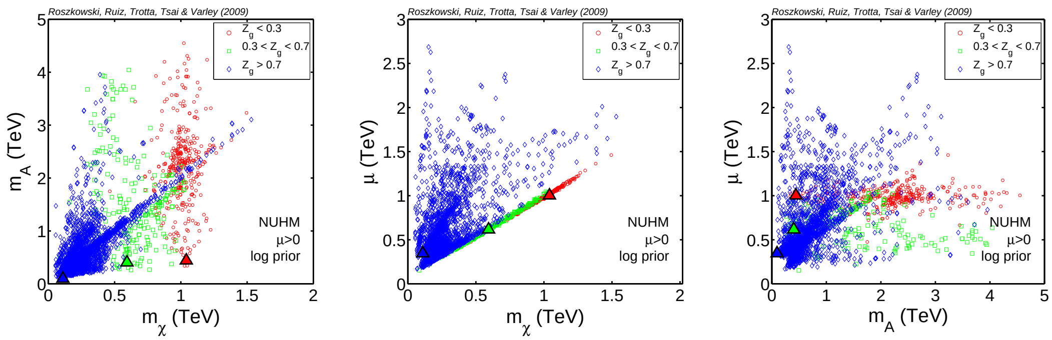

Figure 8: From left to right, values of the gaugino fraction Z_g in the planes of: (m_χ, m_A), (m_χ, μ) and (m_A, μ), for samples uniformly selected from our MC chains obtained. The color coding is as before.

completely override the prior choice. Therefore, we also investigate the values of the best-fit χ^2 values in each of the three regions separately, see Table 3. The overall best-fit is in the region where the LSP is mostly gaugino, where the $\chi^2 = 1.6$. The value increases to $\chi^2 = 10.52$ for the best-fit in the mixed region, and to $\chi^2 = 12.12$ for the higgsino region. Therefore, from the point of view of a goodness-of-fit test, the higgsino region would appear to be completely excluded. However, the detailed breakdown of the total χ^2 into the contribution from each observable reveals that most of the penalty for the best-fit points in the mixed and higgsino region comes from $(g-2)_\mu$, see bottom section of Table 3. In fact, it is only in the bino region that an excellent fit to the observed anomalous magnetic moment can be achieved. This has a very simple physical explanation, namely the fact that the region where the neutralino is mostly bino is in the bulk region, hence the value of the SUSY masses is low.

If one removes $\delta(g-2)_\mu$ from the analysis, we find that the best-fit χ^2 values for the three different regions become very close to each other: $\chi^2 = 1.60, 2.42, 2.32$ for the bino, mixed and higgsino regions, respectively. With a $\Delta\chi^2 \lesssim 0.8$ wrt the overall best-fit, the best-fit higgsino DM point can no longer be ruled out even at the 1σ level if one removes the $(g-2)_\mu$ constraint. This demonstrates that the overall best-fit value and the profile likelihood maps are being driven to a large extent by the (somewhat controversial) $\delta(g-2)_\mu$ constraint. We stress once more at this point, however, that the best-fit values found above in each region have been derived from our MCMC samples, and therefore they cannot be considered as necessarily being the global best fits that could be obtained with a dedicated algorithm, optimized for likelihood maximisation. We can however consider those points as representative of the quality of fit in each region.

At the same time, all three regions achieve very satisfactory fits of the WMAP relic abundance, albeit via quite different physical mechanisms. In the mixed case, annihilation to gauge bosons is required to give the right relic density, while for higgsino domination there are coannihilation processes with the next-to-lightest neutralino and the lightest chargino, along with $t\bar{t}$ and gauge boson pair final states contributing to the required reduction of the relic DM density. This is a consequence of the masses of the lightest chargino and of the two lightest neutralinos becoming very close to each other. Indeed, the two most important annihilation channels reported in Table 1 for the higgsino best-fit point are only just ahead of about a dozen coannihilation-based processes.

In summary, the parameters of the NUHM exhibit a rather complex structure, with different regions of parameter space leading to very different DM compositions. We have identified two dominant regimes: one corresponds mostly to large values of the soft mass parameters and gives a ~ 1 TeV higgsino-like neutralino, while the other is more similar to the situation seen in the CMSSM, with bino dark matter and a lighter spectrum. In between the two there is a fairly statistically insignificant number of cases corresponding to a rather quick transition between the higgsino and bino dominated DM compositions. Our detailed statistical analysis finds that the latter scenario is favoured, although it is not possible to rule out robustly the former possibility. In particular, we have found that the difference in the best-fit χ^2 for the two cases is largely due to the $(g-2)_\mu$ constraint, and as such it should be evaluated with some care.

4. Direct and indirect dark matter detection signatures

We now proceed to examine implications from our global scans for the detection of the lightest neutralino as dark matter, considering both direct detection via its elastic scatterings with targets in underground detectors, as well as indirect signatures of neutralino pair annihilation resulting in an additional component of diffuse gamma radiation from the Galactic center and of positron flux from the Galactic halo. The underlying formalism for both direct and indirect search modes can be found in several sources. (See, e.g., [41, 42, 43, 44].) In our analysis we have followed the procedure as well as hadronic matrix elements inputs as presented in our earlier work [14, 26, 45]. Some investigations into this area in the case of non-universality have also been done in the literature, see for example refs. [7, 46].

4.1 Direct detection prospects

Fig. 9 shows some quantities of interest in the plane spanned by the spin-independent cross section σ_p^{SI} and the neutralino mass m_χ. The left panel shows 68% and 95% contours from the 2D posterior pdf, with uniformly weighted samples from the posterior colour-coded according to the neutralino composition. The right panel shows the profile likelihood instead. For comparison, some of the most stringent 90% CL experimental upper limits are also superimposed [47, 48, 49]. Due to the significant uncertainties in comparing theoretical predictions with experimental direct detection limits, we have chosen not to impose those limits in the likelihood at this stage. However, current constraints are starting to impinge on the favoured parameter space region, whose structure and extent is fairly similar to what is found in the CMSSM [19]. From the direct detection point of view, therefore, there is little else than the ~ 1 TeV higgsino-like WIMP to tell the two models apart. We also note that in terms of the posterior pdf all of the 68% probability region (inner contours) lies above $\sigma_p^{SI} \gtrsim 10^{-10}$ pb which means that the favoured spin-independent cross section region in the NUHM will be basically completely explored by future 1-tonne detectors whose sensitivity reach is likely to be of that order or better. This is encouraging in terms of being able to probe experimentally the favoured parameter space of the model. As can be seen from the right panel of Fig. 9 , the profile likelihood result essentially singles out a favoured region at small neutralino mass and cross section between some 10^{-10} and 10^{-8} pb. The higgsino-like region (red swarm of points in the left-hand panel) appears ruled out in terms of the profile likelihood, but as noted above this is mostly due to the $(g-2)_\mu$ constraint.

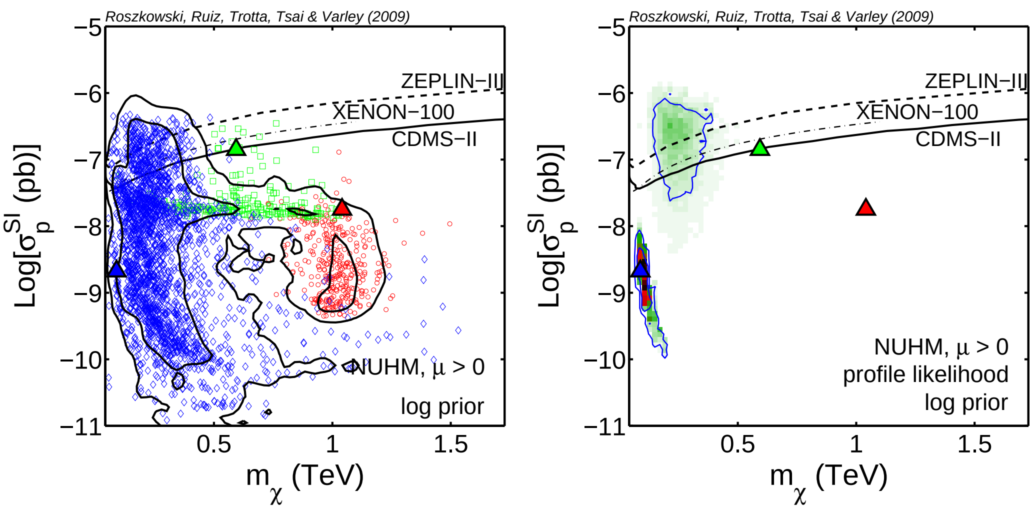

Figure 9: Left panel: favoured regions (black contours, enclosing 68% and 95% probability) for the dark matter spin-independent cross section σ_p^{SI} *vs.* the neutralino mass m_χ in the NUHM model, together with some recent experimental upper limits (which have not been enforced in the likelihood). Samples from the posterior are plotted in different colours, highlighting regions of different DM composition: blue for gaugino-like, red for higgsino-like and green for the mixed type. The triangles denote the location of the best-fit points in each region. Right panel: profile likelihood for the same variables.

4.2 Indirect detection

Next we discuss some indirect detection modes of much current interest. We follow the formalism and procedure outlined in ref. [45] which we briefly summarize here for completeness. In our numerical analysis we rely on DarkSusy [25] to compute the fluxes. To start with, we compute the total γ-ray flux Φ_γ produced by dark matter annihilations in the Galactic halo,

$$\Phi_\gamma(\Delta\Omega) = \int_{E_{\rm th}}^{m_\chi} dE_\gamma \, d\Phi_\gamma/dE_\gamma(E_\gamma, \Delta\Omega), \tag{4.1}$$

where the cone $\Delta\Omega$ is centered on the direction ψ and the integration goes over the range of photon energies from an energy threshold $E_{\rm th}$ up to m_χ. The differential diffuse γ–ray flux arriving from a direction at an angle ψ from the Galactic center is given by

$$\frac{d\Phi_\gamma}{dE_\gamma}(E_\gamma, \psi) = \sum_i \frac{\sigma_i v}{8\pi m_\chi^2} \frac{dN_\gamma^i}{dE_\gamma} \int_{\rm l.o.s.} dl \, \rho_\chi^2(r(l, \psi)), \tag{4.2}$$

where $\sigma_i v$ is a product of the WIMP pair-annihilation cross section into a final state i times the pair's relative velocity and dN_γ^i/dE_γ is the differential γ–ray spectrum (including a branching ratio into photons) following from the state i. Here we consider contributions from the continuum (as opposed to photon lines coming from one loop direct neutralino annihilation into $\gamma\gamma$ and γZ), resulting from cascade decays of all kinematically allowed final state SM fermions and combinations of gauge and Higgs bosons. The integral is taken along the line of sight (l.o.s.) from the detector. It is convenient to separate factors depending on particle physics and on halo properties by introducing the dimensionless quantity $J(\psi) \equiv (1/8.5\,\mathrm{kpc})\left(0.3\ \mathrm{GeV/cm^3}\right)^2 \int_{\mathrm{l.o.s.}} dl\, \rho_\chi^2(r(l,\psi))$ [50]. The flux is further averaged over the solid angle $\Delta\Omega$ representing the acceptance angle of the detector, and one defines the quantity $\bar{J}(\Delta\Omega) = (1/\Delta\Omega)\int_{\Delta\Omega} J(\psi) d\Omega$. Since we are interested in the Galactic center, we set $\psi = 0$.

The flux from the Galactic center critically depends on the dark matter halo profile at small Galactic radius r where dark matter density is thought to be largest. In this analysis, as also previously in [45], we consider the NFW model [51],

$$\rho_\chi(r) = \frac{\rho_s}{(r/r_s)[1+(r/r_s)]^2}, \tag{4.3}$$

where $\rho_s = 0.285\ \mathrm{GeV/cm^3}$ and $r_s = 20.0\,\mathrm{kpc}$, motivated by results from past numerical simulations [52, 53]. In addition also include the Einasto model which has recently become more favored by numerical simulations of galactic halos [54, 55],

$$\rho(r) = \rho_s \exp\{\left[\frac{2}{\alpha}\frac{r_s^\alpha - r^\alpha}{r_s^\alpha}\right]\}, \tag{4.4}$$

which has recently become favored by numerical simulations of the Galactic halo. We adopt (thereafter called "Einasto") with parameters $\rho_s = 0.054\ \mathrm{GeV/cm^3}$, the scale radius $r_s = 21.5\,\mathrm{kpc}$ and best-fit case for the slope $\alpha = 0.17$ [56]. The inner radius density profile for Einasto profile is not as steep as the NFW one with r^{-1}. Close to solar radius both models become quite similar.

In fig. 10 we present our predictions for the diffuse γ-ray flux Φ_γ produced by dark matter annihilation in the Galactic center *vs.* the neutralino mass m_χ for the NFW halo model. We also assume a conservative energy threshold $E_{\mathrm{th}} = 10$ GeV and $\Delta\Omega = 10^{-5}$sr to match Fermi's resolution. Both the 68% and the 95% total probability ranges (inner and outer contours, respectively) are shown. As expected, the largest flux corresponds to the low-mass bino-like neutralino region, but note the 68% probability the higgsino-like region at $m_\chi \sim 1$ TeV. Blue, red and green trianges denote the best-fit points for the bino, mixed and higgsino-like cases, as before. Fermi's reach with one year of data is also indicated (horizontal black/dashed line [57]). Using the Einasto model instead gives slightly lower fluxes, since the profile is less steep in the Galactic center than the NFW one.

The emerging picture is fairly similar to the CMSSM [45]. In particular, it is clear that the largest uncertainty in assessing Fermi's prospects for detecting a signal in this model lies in the cuspiness of the dark matter halo profile at small radii. If the steepness of the profile in the Galactic center is similar to that of the NFW or Einasto model, then a signal in the NUHM or CMSSM is highly unlikely.

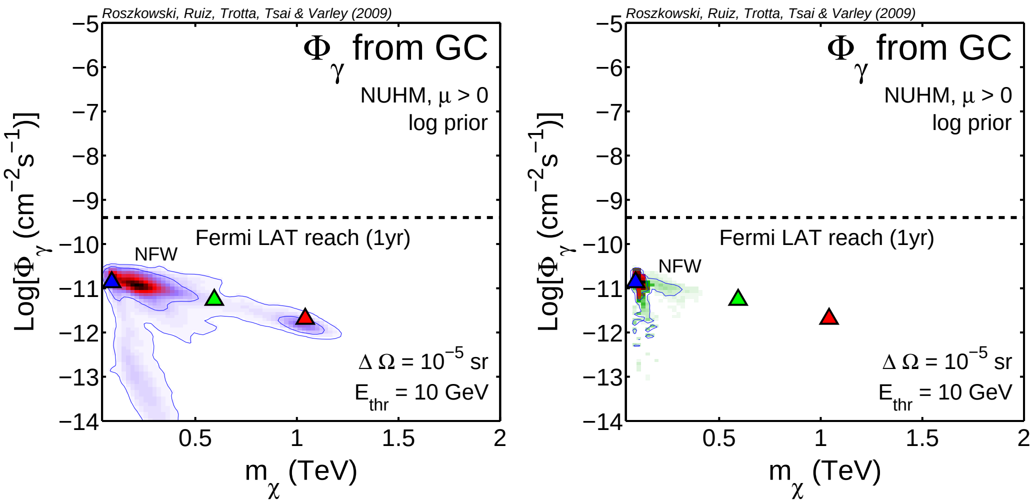

Figure 10: The diffuse γ-ray flux Φ_γ above 10 GeV produced by dark matter annihilation in the Galactic center *vs.* the neutralino mass m_χ for some popular halo models. The left panel shows the posterior pdf (with 68% and 95% regions), while the right panel presents the profile likelihood.

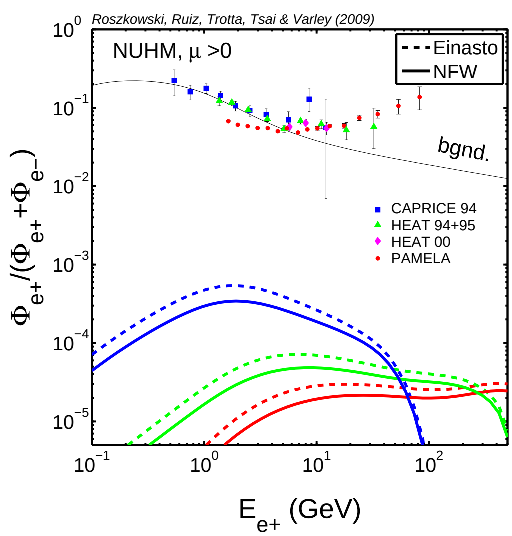

Figure 11: Positron flux fraction produced by dark matter annihilation in the Galactic halo *vs.* the positron energy E_{e^+}, for the three best-fit points corresponding to different DM composition: gaugino (blue), mixed (green) and higgsino (red). The solid lines assume the NFW profile, while the dashed lines are for the Einasto profile. Everywhere a boost factor BF=1 is assumed.

Finally we present the NUHM's predictions for positron flux from neutralino dark matter annihilation in the local halo. Once produced, positrons propagate through the Galactic medium and their spectrum is distorted due to synchrotron radiation and inverse Compton scattering at high energies, bremsstrahlung and ionization at lower energies. The effects of positron propagation are computed following a standard procedure described in [58, 59], by solving numerically the diffusion-loss equation for the number density of positrons per unit energy $dn_{e^+}/d\varepsilon$. The diffusion coefficient is parameterized as $K(\varepsilon) = K_0(3^\alpha + \varepsilon^\alpha)$, with $K_0 = 2.1 \times 10^{28}$ cm^{2}sec^{-1}, $\alpha = 0.6$ and $\varepsilon = E_{e^+}/1$ GeV, mimicking re-acceleration effects. The energy loss rate is given by $b(\varepsilon) = \tau_E \varepsilon^2$, with $\tau_E = 10^{-16}$sec^{-1}, and we describe the diffusion zone (i.e., the Galaxy) as an infinite slab of height $L = 4$ kpc, with free escape boundary conditions. Changes in the above positron propagation model, especially $K(\varepsilon)$ (see, e.g., [60, 59]), can potentially lead to variations by a factor of 5 to 10 in the spectral shape at low positron energy, $E_{e^+} \lesssim 20$ GeV [61]. Most high-energy positrons, on the other hand, originate from the local neighborhood the size of a few kpcs [59, 62], and their flux is less dependent of the halo and propagation dynamics. In order to reduce the impact of solar winds and magnetosphere effects on the model's predictions, it is useful to consider the positron fraction, defined as $\Phi_{e^+}/(\Phi_{e^+} + \Phi_{e^-})$, where Φ_{e^+} is the positron differential flux from WIMP annihilation, while Φ_{e^-} is the background electron flux. For background e^- and e^+ fluxes we follow the parametrization adopted in ref. [59] from ref. [60].

In fig. 11 we present the positron flux fraction produced by dark matter annihilation in the Galactic halo *vs.* the positron energy E_{e^+} for the bino (blue), mixed (green) and higgsino-like (red) cases, and for the two halo models considered above. Also included are the relevant experimental data [63, 64], including the recent Pamela result. It is clear that supersymmetric dark matter in the models like the NUHM (and also the CMSSM [45]) falls far short of reproducing the Pamela result. This would remain true even if one would be prepared to consider an unlikely existence of very dense local DM clumps for which the boost factor would be unrealistically high, $\sim 10^3$. Although a more refined analysis fitting signal and background simultaneously would be required to draw more quantitative conclusions, it is clear that the spectrum predicted by the NUHM appears to have a very different energy dependence from the flux observed by Pamela. This is not necessarily a problem for the NUHM, and other unified SUSY models like the CMSSM, as long as their signal remains below the observed flux, since a more conventional astrophysical explanation in terms of pulsar radiation may be entirely sufficient to account for Pamela observations [65].

5. Conclusions

The MCMC analysis of the Non-Universal Higgs Model performed in this paper reveals a remarkably rich and complex structure of its parameter space. While the properties of the model are in some aspects fairly similar to the CMSSM, we have found several interesting differences. Perhaps the biggest one is the existence of higgsino-like dark matter with a mass close to 1 TeV. The higgsino dark matter results from having more parameters than in the CMSSM but also from the focusing effect being less strong than in that model. A detailed statistical analysis shows that this higgsino-like DM region is put under pressure essentially only by the constraint from the anomalous magnetic moment of the muon, while all other present-day constraints cannot rule out this possibility very strongly.

In terms of observational consequences at colliders, while a more detailed analysis would be required to make a more rigorous quantitative statement, a simple comparison of the mass spectra of the superpartners and the lightest Higgs leads us to believe that the NUHM appears rather similar to the CMSSM, which will make it difficult to experimentally distinguish the two models. Again, the best prospects may be provided by finding in direct detection searches a ~ 1 TeV dark matter WIMP, since such a case in the CMSSM is highly unlikely [26, 19]. Fermi's prospects for probing the model strongly depend on the cuspiness of the dark matter profile in the Galactic center, and with NFW-like profiles appear rather unimpressive. Likewise, positrons produced in dark matter annihilation remain well below the Pamela result.

Acknowledgments

LR is partially supported by the EC 6th Framework Programmes MRTN-CT-2004-503369 and MRTN-CT-2006-035505. RRdA is supported by the project PARSIFAL (FPA2007-60323) of the Ministerio de Educación y Ciencia of Spain. TV is supported by STFC. R.T. would like to thank the Galileo Galilei Institute for Theoretical Physics for the hospitality and the INFN and the EU FP6 Marie Curie Research and Training Network "UniverseNet" (MRTN-CT-2006-035863) for partial support. The authors would like to thank the European Network of Theoretical Astroparticle Physics ENTApP ILIAS/N6 under contract number RII3-CT-2004-506222 for financial support. This project benefited from the CERN-ENTApP joint visitor's programme on dark matter, 2-6 February 2009. The use of the Iceberg computer cluster at the University of Sheffield is gratefully acknowledged.

A. Illustration of prior dependence

We illustrate the dependence of our results on the choice of priors for the NUHM parameters. As in any Bayesian analysis, the choice of priors determines the metric with which the parameter space is scanned, and therefore it can have an impact on the resulting posterior probabilities. It is however expected that the prior choice ought to become irrelevant once the constraining power of the data is sufficient (see [66] for an illustration). Indeed, it has been shown in a case study that future LHC mass spectrum measurements are likely to lead to inferences on the parameters of the CMSSM whose prior dependence will be strongly reduced [20].

We repeated our scans using a prior uniform in the NUHM masses ($m_{1/2}$, m_0, m_{H_u} and m_{H_d}), rather than uniform in their log, as before. The prior on the remaining NUHM and SM parameters has been left unchanged. We call this prior choice the *flat prior*. *A priori*, this choice expresses a state of indifference with respect to the masses themselves, rather than with respect to their order of magnitude, as with the log prior. However, one has to bear in mind that a choice of a uniform metric on a linear scale can lead to very strong "volume effects" even in a parameter space of moderate dimensionality. This refers to the fact that on a linear scale most of the volume of a D dimensional cube is near its edges. To estimate the magnitude of this volume effect, recall that, for the flat prior, the volume encompassed by the mass range between e.g. 1 and 4 TeV is a factor 10^4 larger than between 100 and 400 GeV. For comparison, under the log prior the ratio of the volumes of the two regions is unity. Therefore, in order to completely override the prior volume via the likelihood, one would need at least a $\sim 4.3\sigma$ preference for the low mass region. Clearly, current data is not constraining enough to override the prior preference for large mass in this case. Therefore, analogously to what is observed in the CMSSM [19, 13], we expect that under a flat prior choice our posterior probability mass will be shifted towards larger masses.

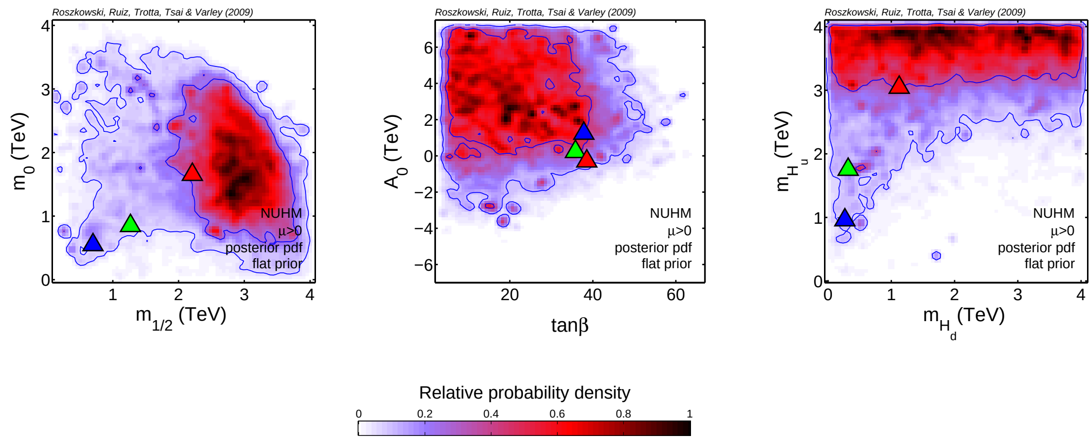

Figure 12: The same as in fig. 1 but for the flat prior. Coloured triangles show the location of the best-fits for each of the DM composition (blue for gaugino, red for higssino and gree for mixed). The considerable shift in the probability density is largely due to a volume effect from the flat prior arising from the large number of samples at large mass for this choice of priors.

This is indeed what is observed in fig. 12, which is to be compared with fig. 1. The overall effect of the flat prior is to produce a large number of samples in the large mass region, despite the fact that the best fit is still found in the low mass region. A closer analysis reveals that the average χ^2 of the 68% probability cloud is rather poor, ($\langle\chi^2\rangle = 20.88$) hence pointing to a strong volume effect. Thus the flat prior appears to override the preference for the small mass region (where the average χ^2 is generally better), in the sense that it imposes a measure on parameter space that does not adequately explore the low mass region.

A detailed comparison of the results from the two prior choices shows that generically the flat prior puts a stronger *a priori* probability to the large mass region, therefore generally favouring more strongly the higgsino-like DM scenario outlined before. Therefore in a flat prior scan all of the distinctive higgsino-like features highlighted above are strongly enhanced. The best-fit χ^2 found under the flat prior is also quite a bit poorer than the one under the log prior: $\chi^2 = 5.55$ under the flat prior vs $\chi^2 = 1.62$ under the log prior. This shows that the flat prior scan does not sample accurately enough the low-mass region, which has a relatively small extension given the choice of a uniform metric on a linear scale. On the other hand, removing the $(g-2)_\mu$ constraint brings the best fit value for the flat prior ($\chi^2 = 2.25$) within less than 1σ of the value obtained for the log prior without the $(g-2)_\mu$ constraint ($\chi^2 = 1.60$), showing that it is indeed this latter measurement that primarily drives the quality of fit in both scans. As mentioned above, this result shows that the best-fit values obtained from our MCMC scans can only be considered as representative of the quality of fit that can be achieved in each region. A dedicated investigation of the robustness of the best-fit values and of the ensuing profile likelihood is left to a future work.

The phenomenology ensuing from the flat prior choice remains qualitatively similar to what has been presented above, although there are fairly evident quantitative differences due to the volume effects mentioned here.

It must be emphasised that the physical features of a model necessarily *do not* depend on our choice of Bayesian prior – in each case a given point in the parameter space will give the same physical result. What does depend on the prior in the case of insufficiently constraining data is the weighting that a given point contributes to producing a posterior, which is a probabilistic and not physical result. Therefore, while the physical signatures for a given model are obviously prior independent, the ensuing statistical conclusions may, and often do, depend on the choice of priors and statistical approach used. Of course in the limit of strongly constraining data, statistical inferences are expected to become essentially independent of such choices. While we point out that current data are not sufficiently constraining to eliminate prior dependence in the NUHM, we do consider our results obtained under the log prior to be more robust and more conservative.

References

[1] See, e.g., H. E. Haber and G. L. Kane, *The Search for Supersymmetry: Probing Physics Beyond the Standard Model Phys. Rept.* **117** (1985) 75;
S. P. Martin, *A Supersymmetry Primer*, [hep-ph/9709356].

[2] G. L. Kane, C. F. Kolda, L. Roszkowski and J. D. Wells, *Study of constrained minimal supersymmetry*, *Phys. Rev.* **D 49** (1994) 6173 [hep-ph/9312272].

[3] T. Blazek, R. Dermisek and S. Raby, *Predictions for the Higgs and supersymmetry spectra from SO(10) Yukawa unification with μ greater than 0* , *Phys. Rev. Lett.* **88** (2002) 111804 [hep-ph/0107097]; and *Yukawa unification in SO(10)*, *Phys. Rev.* **D 65** (2002) 115004 [hep-ph/0201081].

[4] R. Dermisek, S. Raby, L. Roszkowski and R. Ruiz De Austri, *Dark matter and $B(s) \to \mu^+\mu^-$ SO(10) soft susy breaking*, *J. High Energy Phys.* **037** (2003) 0304 [hep-ph/0304101]; *Dark matter and $B(s) \to \mu^+\mu^-$ SO(10) soft susy breaking II*, *J. High Energy Phys.* **029** (2005) 0509 [hep-ph/0507233].

[5] See, e.g., V. Berezinsky, et al.*Neutralino dark matter in supersymmetric models with non-universal scalar mass terms*, Astropart. Phys. **5** (1996) 1 [hep-ph/9508249];
P. Nath and R. L. Arnowitt, *Non-universal soft SUSY breaking and dark matter*, Phys. Rev. D **56** (1997) 2820 [hep-ph/9701301];
M. Drees, et al., *Light Higgsino dark matter*, Phys. Rev. D **56** (1997) 276 [Erratum-ibid. D **64** (2001) 039901] [hep-ph/9701219].

[6] H. Baer, et al., *Neutralino cold dark matter in a one parameter extension of the minismal supergravity model*, Phys. Rev. D **71** (2005) 095008 [hep-ph/0412059].

[7] H. Baer, et al., *Direct, indirect and collider detection of neutralino dark matter in SUSY models with non-universal Higgs masses*, *J. High Energy Phys.* **0507** (2005) 065 [hep-ph/0504001].

[8] J. R. Ellis, K. A. Olive and Y. Santoso, *The MSSM Parameter Space with Non-Universal Higgs Masses*, Phys. Lett. B **539** (2002) 107 [hep-ph/0204192].

[9] J. R. Ellis, T. Falk, K. A. Olive and Y. Santoso, *Exploration of the MSSM with Non-Universal Higgs Masses*, Nucl. Phys. B **652** (2003) 259 [hep-ph/0210205].

[10] J. R. Ellis, S. F. King and J. P. Roberts, *The Fine-Tuning Price of Neutralino Dark Matter in Models with Non-Universal Higgs Masses*, *J. High Energy Phys.* **0804** (2008) 099 [hep-ph/0711.2741].

[11] H. Baer, et al., *Collider signals and neutralino dark matter detection in relic-density-consistent models without universality*, *J. High Energy Phys.* **0805** (2008) 058 [hep-ph/0802.3384].

[12] J. R. Ellis, et al., *Charginos and Neutralinos in the Light of Radiative Corrections: Sealing the Fate of Higgsino Dark Matter*, Phys. Rev. D **58** (1998) 095002 [hep-ph/9801445];
J. R. Ellis, et al., *Supersymmetric Dark Matter in the Light of LEP and the Tevatron Collider*, Phys. Rev. D **62** (2000) 075010 [hep-ph/0004169].

[13] B. C. Allanach and C. G. Lester, *Multi-dimensional MSUGRA likelihood maps*, *Phys. Rev.* **D 73** (2006) 015013 [hep-ph/0507283];
B. C. Allanach, *Naturalness priors and fits to the constrained minimal supersymmetric standard model*, *Phys. Lett.* **B 635** (2006) 123 [hep-ph/0601089];
B. C. Allanach, C. G. Lester and A . M. Weber, *The dark side of mSUGRA*, *J. High Energy Phys.* **0612** (2006) 065 [hep-ph/0609295].

[14] R. Ruiz de Austri, R. Trotta and L. Roszkowski, *A Markov Chain Monte Carlo analysis of the CMSSM*, *J. High Energy Phys.* **0605** (2006) 002 [hep-ph/0602028]; see also R. Trotta, R. Ruiz de Austri and L. Roszkowski, *Prospects for direct dark matter detection in the Constrained MSSM*, New Astron. Rev. **51** (2007) 316-320, [astro-ph/0609126].

[15] O. Buchmueller, et al., *Predictions for Supersymmetric Particle Masses in the CMSSM using Indirect Experimental and Cosmological Constraints*, [hep-ph/0808.4128] and *Likelihood Functions for Supersymmetric Observables in Frequentist Analyses of the CMSSM and NUHM1*, O. Buchmueller, et al., Eur.Phys.J.C64:391-415,2009 [hep-ph/0907.5568].

[16] See: http://www.superbayes.org/

[17] L. Roszkowski, R. Ruiz de Austri and R. Trotta, *On the detectability of the CMSSM light Higgs boson at the Tevatron*, *J. High Energy Phys.* **0704** (2007) 084 [hep-ph/0611173].

[18] F. Feroz, et al., *Bayesian Selection of sign(mu) within mSUGRA in Global Fits Including WMAP5 Results*, *J. High Energy Phys.* **10** (2008) 064

[19] R. Trotta, et al., *The impact of priors and observables on parameter inferences in the Constrained MSSM*, *J. High Energy Phys.* **0812** (2008) 024 [hep-ph/0809.3792].

[20] L. Roszkowski, R. Ruiz de Austri and R. Trotta, *Efficient reconstruction of CMSSM parameters using LHC data - A Case Study*, [hep-ph/0907.0594]

[21] Y. Akrami, et al., *A Profile Likelihood Analysis of the Constrained MSSM with Genetic Algorithms*, JHEP **1004** (2010) 057 [hep-ph/0910.3950].

[22] M. Bridges, K. Cranmer, F. Feroz, M. Hobson, R. R. de Austri and R. Trotta, arXiv:1011.4306 [hep-ph]; Y. Akrami, C. Savage, P. Scott, J. Conrad and J. Edsjo, arXiv:1011.4297 [hep-ph].

[23] F. Feroz et al., in preparation.

[24] B. C. Allanach, *SOFTSUSY: a C++ program for calculating supersymmetric spectra*, *Comput. Phys. Commun.* **143** (2002) 305 [hep-ph/0104145].

[25] P. Gondolo, et al., *DARKSUSY: computing supersymmetric dark matter properties numerically*, *JCAP* **0407** (2004) 008 [astro-ph/0406204]; http://www.physto.se/edsjo/darksusy/.

[26] L. Roszkowski, R. Ruiz de Austri and R. Trotta, *Implications for the Constrained MSSM from a new prediction for b to s gamma*, *J. High Energy Phys.* **0707** (2007) 075, [hep-ph/0705.2012].

[27] F. Feroz and M. P. Hobson *Multimodal nested sampling: an efficient and robust alternative to MCMC methods for astronomical data analysis*, Mon. Not. Roy. Astron. Soc. **384** 449 (2008); F. Feroz, M. P. Hobson and M. Bridges, *MultiNest: an efficient and robust Bayesian inference tool for cosmology and particle physics* (2008), [astro-ph/0809.3437]

[28] Tevatron Electroweak Working Group (for the CDF and D0 Collaborations), *A Combination of CDF and D0 Results on the Mass of the Top Quark*, [hep-ex/0703034].

[29] W.-M. Yao et al. [Particle Data Group], *J. Phys.* **G33** (2006) 1.

[30] See http://lepewwg.web.cern.ch/LEPEWWG.

[31] K. Hagiwara, A. D. Martin, D. Nomura and T. Teubner, *Improved predictions for g-2 of the muon and* $\alpha_{\rm QED}(M_Z^2)$, Phys. Lett. B **649** (2007) 173 [hep-ph/0611102].

[32] Heavy Flavor Averaging Group (HFAG) (E. Barberio et al.), *Averages of b-hadron properties at the end of 2005*, [hep-ex/0603003]; for a more recent update see Heavy Flavor Averaging Group (HFAG) (E. Barberio et al.), *Averages of b-hadron properties at the end of 2006*, [hep-ex/0704.3575].

[33] The CDF Collaboration, *Measurement of the* $B_s - \bar{B}_s$ *oscillation frequency*, *Phys. Rev. Lett.* **97** (2006) 062003 [hep-ex/0606027]. and *Observation of* $B_s - \bar{B}_s$ *oscillations*, *Phys. Rev. Lett.* **97** (2006) 242003 [hep-ex/0609040].

[34] E. Komatsu, et al.[WMAP Collaboration], *Five-Year Wilkinson Microwave Anisotropy Probe (WMAP) Observations:Cosmological Interpretation*, Astrophys. J. Suppl. **180** (2009) 330 [astro-ph/0803.0547].

[35] T. Aaltonen, etal [CDF Collaboration], *Search for* $B_s \to \mu^+\mu^-$ *and* $B_d \to \mu^+\mu^-$ *Decays with* $2fb^{-1}$ *of* $p\bar{p}$ *Collisions*, Phys. Rev. Lett. **100** (2008) 101802 [hep-ex/0712.1708].

[36] The LEP Higgs Working Group, http://lephiggs.web.cern.ch/LEPHIGGS; G. Abbiendi et al. [the ALEPH Collaboration, the DELPHI Collaboration, the L3 Collaboration and the OPAL Collaboration, The LEP Working Group for Higgs Boson Searches], *Search for the standard model Higgs boson at LEP*, *Phys. Lett.* **B 565** (2003) 61 [hep-ex/0306033].

[37] B. C. Allanach, K. Cranmer, C. G. Lester and A. M. Weber, *Natural Priors, CMSSM Fits and LHC Weather Forecasts*, *J. High Energy Phys.* **0708** (2007) 023 [arXiv:0705.0487].

[38] F. Feroz, M. P. Hobson, L. Roszkowski, R. Ruiz de Austri and R. Trotta, *Are BR($b \to s\gamma$) and $(g-2)_\mu$ consistent within the Constrained MSSM?* , [hep-ph/0903.2487].

[39] M. Olechowski and S. Pokorski, *Electroweak symmetry breaking with nonuniversal scalar soft terms and large tan beta solutions*, Phys. Lett. B **344** (1995) 201 [hep-ph/9407404].

[40] K. L. Chan, U. Chattopadhyay and P. Nath, *Naturalness, Weak Scale Supersymmetry and the Prospect for the Observation of Supersymmetry at the Tevatron and at the LHC*, *Phys. Rev.* **D 58** (1998) 096004 [hep-ph/9710473];
J. L. Feng, K. T. Matchev and T. Moroi, *Multi - TeV scalars are natural in minimal supergravity*, *Phys. Rev. Lett.* **84** (2000) 2322 [hep-ph/9908309];
Focus points and naturalness in supersymmetry, *Phys. Rev.* **D 61** (2000) 075005 [hep-ph/9909334];
J. L. Feng, K. T. Matchev and F. Wilczek, *Neutralino dark matter in focus point supersymmetry*, *Phys. Lett.* **B B482** (2000) 388 [hep-ph/0004043].

[41] M. Drees and M. Nojiri, *Neutralino - nucleon scattering revisited*, *Phys. Rev.* **D 48** (1993) 3483 [hep-ph/9307208].

[42] See, e.g., G. Jungman, M. Kamionkowski and K. Griest, *Supersymmetric dark matter*, *Phys. Rept.* **267** (1996) 195;
C. Muñoz, *Dark Matter Detection in the Light of Recent Experimental Results*, *Int. J. Mod. Phys.* **A 19** (2004) 3093 [hep-ph/0309346].

[43] J. Ellis, A. Ferstl, K. A. Olive, *Reevaluation of the elastic scattering of supersymmetric dark matter*, *Phys. Lett.* **B 481** (2000) 304 [hep-ph/0001005].

[44] Y. G. Kim, T. Nihei, L. Roszkowski and R. Ruiz de Austri, *Upper and lower limits on neutralino WIMP mass and spin-independent scattering cross section, and impact of new (g-2)(mu) measurement*, *J. High Energy Phys.* **0212** (2002) 0342002 [hep-ph/0208069].

[45] L. Roszkowski, R. R. de Austri, J. Silk and R. Trotta, *On prospects for dark matter indirect detection in the Constrained MSSM*, Phys. Lett. B **671**, 10 (2009) [astro-ph/0707.0622].

[46] Y. Mambrini and C. Munoz, *Gamma-ray detection from neutralino annihilation in non-universal SUGRA scenarios*, Astropart. Phys. **24** (2005) 208 [hep-ph/0407158].

[47] V. N. Lebedenko, et al., *Result from the First Science Run of the ZEPLIN-III Dark Matter Search Experiment*, [astro-ph/0812.1150].

[48] E. Aprile, et al.[XENON100 Collaboration], *First Dark Matter Results from the XENON100 Experiment*, [astro-ph.CO/1005.0380].

[49] Z. Ahmed, et al.[The CDMS-II Collaboration], *Results from the Final Exposure of the CDMS II Experiment*, [astro-ph.CO/0912.3592].

[50] L. Bergström, P. Ullio and J. Buckley, *Observability of Gamma Rays from Dark Matter Neutralino Annihilations in the Milky Way Halo*, *Astropart. Phys.* **9** (1998) 137 [astro-ph/9712318].

[51] J. F. Navarro, C. S. Frenk and S. D. M. White, *The structure of cold dark matter halos*, *Astrophys. J.* **462** (1996) 563 [astro-ph/9508025] and *A universal density profile from hierarchical clustering*, *Astrophys. J.* **490** (1997) 493.

[52] J. F. Navarro, et al., Mon. Not. Roy. Astron. Soc. **349** (2004) 1039 [arXiv:astro-ph/0311231].

[53] A. W. Graham, et al. "Empirical models for Dark Matter Halos. I. Nonparametric Construction of Density Profiles and Comparison with Parametric Models," Astron. J. **132**, 2685 (2006) [arXiv:astro-ph/0509417].

[54] J. Einasto, Trudy Inst. Astroz. Alma-Ata, 51, 87, 1965.

[55] J. F. Navarro, et al., [astro-ph/0810.1522].

[56] J. Diemand, et al., "Clumps and streams in the local dark matter distribution," arXiv:0805.1244 [astro-ph].

[57] See: `http://tinyurl.com/yp6g5w` (as of Dec 2007).

[58] J. Edsjö, M. Schelke and P. Ullio, *Direct versus indirect detection in mSUGRA with self-consistent halo models*, *JCAP* **0409** (2004) 004 [astro-ph/0405414].

[59] E. A. Baltz and J. Edsjö, *Positron Propagation and Fluxes from Neutralino Annihilation in the Halo*, *Phys. Rev.* **D 59** (1999) 023511 [astro-ph/9808243].

[60] I. V. Moskalenko and A. W. Strong, *Production and propagation of cosmic ray positrons and electrons*, *Astrophys. J.* **493** (1998) 694 [astro-ph/9710124]; I. V. Moskalenko, et al., *Developing the Galactic diffuse emission model for the GLAST Large Area Telescope*, [astro-ph/0704.1328].

[61] D. Hooper and J. Silk, *Searching for Dark Matter with Future Cosmic Positron Experiments*, *Phys. Rev.* **D 71** (2005) 083503 [`hep-ph/0409104`].

[62] J. Lavalle, J. Pochon, P. Salati and R. Taillet, *Clumpiness of Dark Matter and Positron Annihilation Signal: Computing the odds of the Galactic Lottery*, [astro-ph/0603796].

[63] M. A. DuVernois, et al., *Cosmic ray electrons and positrons from 1-GeV to 100-GeV: Measurements with HEAT and their interpretation*, Astrophys. J. **559** (2001) 296.

[64] O. Adriani, et al., *Observation of an anomalous positron abundance in the cosmic radiation*, [astro-ph/0810.4995].

[65] D. Hooper, P. Blasi and P. D. Serpico, *Pulsars as the Sources of High Energy Cosmic Ray Positrons*, JCAP **0901** (2009) 025 [astro-ph/0810.1527]; S. Profumo, *Dissecting Pamela (and ATIC) with Occam's Razor: existing, well-known Pulsars naturally account for the 'anomalous' Cosmic-Ray Electron and Positron Data*, [astro-ph/0812.4457].

[66] R. Trotta, *Bayes in the sky: Bayesian inference and model selection in cosmology*, *Contemporary Physics*, **49**, 2, 71-104 (2008) [astro-ph/0803.4089]